Intramolecular Nitro-Assisted Proton Transfer in Photoirradiated 2-(2′,4′-Dinitrobenzyl)pyridine: Polarized Optical Spectroscopic Study and Electronic Structure Calculations

Panče Naumov,*[,†,‡,§] Kenji Sakurai,[||] Tadahiko Ishikawa,[‡] Junichi Takahashi,[§,⊥] Shin-ya Koshihara,[‡,§] and Yuji Ohashi[‡]

ICYS, National Institute for Materials Science, 1-1 Namiki, Tsukuba, Ibaraki 305-0044, Japan, Tokyo Institute of Technology, 1-12-1 Ookayama, Meguro-ku, Tokyo 152-8551, Japan, Exploratory Research for Advanced Technology (ERATO), 4-1-8 Honcho, Kawaguchi, Saitama 332-0012, Japan, Materials Engineering Laboratory, National Institute for Materials Science, 1-2-1 Sengen, Tsukuba, Ibaraki 305-0047, Japan, and High Energy Accelerator Research Organization (KEK), 1-1 Oho, Tsukuba, Ibaraki 305-0801, Japan

Received: April 20, 2005; In Final Form: June 17, 2005

The nitro-assisted proton transfer (NAPT), responsible for the photoactivity of *ortho*-nitrobenzylpyridines and a model for the nitro-based caged compounds, is studied along with the parent compound 2-(2′,4′-dinitrobenzyl)pyridine (DNBP) with polarized optical spectroscopy and theoretical calculations. The transition dipole moments of a DNBP single-crystal identified oriented molecules of the long-lived enamine tautomer (**NH**), rather than of the aci-nitro tautomer (**OH**), as carriers of the photoinduced blue coloration. It is clarified that the blue second singlet transition owes to intramolecular charge transfer from the allyl-pyridinium part to the dinitrophenyl fragment of **NH**. The theoretical modeling of the ground-state potential energy surface showed that while **NH** and **OH** can interconvert by means of direct proton transfer, such a process between the initial form **CH** and either **OH** and **NH** would require significant rotation of the aromatic rings. In the ground state, **OH** is less stable but the kinetically preferred product over **NH**. Once created, regardless of whether via ground-state or excited-state routes, the aci-nitro group of **OH** undergoes energetically inexpensive rotation to deliver the proton to the nitrogen acceptor. The "softening" of the energy surface around **OH** due to its structural flexibility, that is, mediation of the proton transfer by the nitro group, is crucial to overcome the high barrier for a direct proton jump from **CH** to **NH**, even in cases of unfavorable donor−acceptor geometry. The very small structural change experienced by the surrounding of a molecule undergoing NAPT is promising for the design of photoactive systems which retain their crystallinity during a prolonged operation.

1. Introduction

The solid-state molecular dynamics represents the basis of many interesting physical phenomena. Known motions of molecules in crystals include flips of aromatic rings around a 2-fold axis,[1,2] partial molecular rotations,[3] tumbles, spins, and flips,[4,5] wobbles and spins,[6,7] pedal-like intramolecular rotations,[8−14] reorientations of groups with pseudoconical symmetry,[15,16] in-plane rotations of planar disklike molecules,[17] and overall molecular rotations of spherical molecules.[18,19] The minute geometrical changes of the individual molecules are usually coupled with changes in the physical properties, and sometimes even with an alteration of the chemical identity of the bulk material. Therefore, understanding of the fundamental mechanisms of motions in a crystalline state on a molecular level is a starting point in finding the means for external control of the properties of the materials.

Owing to the vast amount of known nitro compounds, one of the most common dynamic processes in any physical state is the rotation of the nitro group. Although the dynamics of the nitro group, usually detected as increased displacement parameters in crystal structures determined at sufficiently high temperatures, does not significantly affect the rest of the molecular structure, it became clear recently that the enhanced rotation of nitro groups can be responsible for some very important processes, such as the photochromism of the *ortho*-nitrobenzylpyridines (oNBPs). The oNBP moiety is a convenient model for the *ortho*-nitrobenzyl alcohol derivatives (ester carbonates and carbamates) which are the most exploited phototrigger for release of bioactive caged compounds and fluorescent dyes from inactive precursors.[20] Furthermore, it is a prospective switching unit for photon-based optical devices in the macro- and nanoelectronics, due to the large difference of the hyperpolarizibility of its photoisomers.[21] Despite its potentials for application in medicine and photonics, the complete reaction mechanism and the identity of all products of the oNBP group have not been unraveled yet. Photoexcitation at ambient temperatures[22] of the stable colorless form **CH** of oNBP compounds such as the parent molecule 2-(2′,4′-dinitrobenzyl)pyridine (DNBP), in crystalline, molten, solution or dispersed state, results in an intensive blue-violet color (Scheme 1).[23−25] Although the electronic structure of the colorless form

* Corresponding author. Tel.: +81-29-851-3354. Fax: +81-29-860-4706. E-mail: naumov.pance@nims.go.jp. Corresponding author address: ICYS, National Institute for Materials Science, 1-1 Namiki, Tsukuba, Ibaraki 305-0044, Japan.

† National Institute for Materials Science.

‡ Tokyo Institute of Technology.

§ Exploratory Research for Advanced Technology (ERATO).

|| National Institute for Materials Science.

⊥ High Energy Accelerator Research Organization (KEK).

10.1021/jp0520392 CCC: $30.25
Published on Web 07/26/2005

SCHEME 1: Simplified Mechanism of the Main Photo and Thermal Reactions of DNBP (Left) and the Energy Profile of the Reactions of DNBP Compiled and Adapted from Literature Data (Right)[31,32] *a,b*

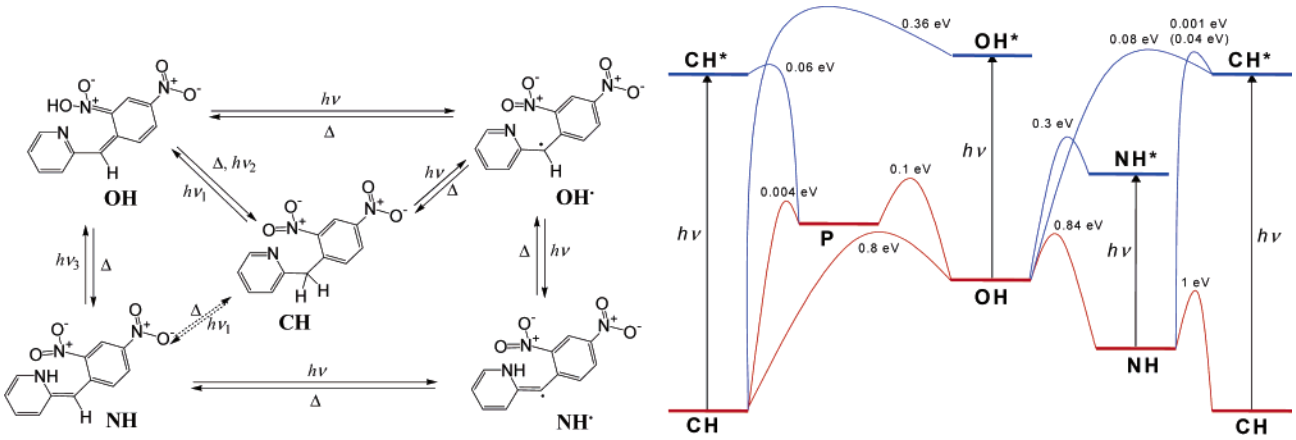

[a] Reactions denoted with broken arrows are characteristic for fluid state. The **NH** form can be created in the solid state, via the **OH** form or the radical reactions. The radical species are created in very small amount compared to the closed-shell species and decay to an array of side products (the complete reaction pathways including the radical species are probably much more complex and are not shown).[22] [b] P denotes a precursor state.

CH of DNBP is known,[26] the detailed electronic structure as well as the origin of the blue species of UV-irradiated oNBPs, usually prescribed to the enamine form **NH**, have not been investigated yet. Furthermore, the nature of the blue species has been often argued, and occasionally it was also attributed to the aci-nitro form **OH** or to both **NH** and **OH**.[27] The spectroscopic measurements in the solid state[25] revealed two different regimes for the creation of **NH** and **OH**: nearly temperature-independent low-yield processes are operative below, while thermally activated processes dominate above ca. 160 and 230 K for **OH** for **NH**, respectively (in the case of DNBP). On the basis of the reaction profile deduced from spectroscopic data[21,24,25] and the structural properties inferred from the diffraction data[28−30] which indicate that a significant part of **NH** is produced from **CH** through **OH**, we have recently suggested a mechanism termed *nitro-assisted proton transfer (NAPT)*[27,28] to explain the mechanistic aspects of the thermally activated proton transfer (PT) reactions in the high-temperature regimes. According to the NAPT, the proton jump is mediated by the photoexcited rotating *ortho*-nitro group via the aci-nitro form **OH** (the pathways **CH↔OH↔NH** in Scheme 1). The NAPT mechanism can explain the polymorph-dependent photoactivity of the oNBPs, which is related to the rotational ability of the nitro group.[30] A unique feature of the NAPT among the solid-state tautomerization reactions is that it can proceed even between an unfavorably oriented donor (CH_2 in **CH**) and an acceptor (pyridyl N in **CH**) without significant perturbation of the long-range structural order. Due to this important characteristic, the oNBP group and the NAPT mechanism seem to be very prospective for incorporation into photonic structures with improved preservation of the crystallinity during prolonged operation. Therefore, a detailed knowledge of the structural and energetic requirements of the NAPT mechanism is essential for future applications.

Several theoretical studies on DNBP also exist. The semiempirical study of the thermal reactions[33] pointed out the relevance of the *ortho*-nitro group for the PT in the crystalline state. Several **CH** and **NH** structures were optimized in the course of the spectroscopic study of DNBP.[34] A Hartree−Fock (HF) and MRD-CI quantum-mechanical treatment[35] considered the lowest excited states of some **CH**, **NH**, and **OH** isomers and the ground-state reaction paths. A first-principles molecular dynamics study of the thermal reactions in gas-phase and solid-state DNBP was also performed.[36]

In this work, to unravel the physical origin of the color change of photoirradiated oNBPs, the electronic structure of the closed-shell photoisomers of DNBP is studied with the linearly-polarized absorption spectra recorded from a blue single crystal. The electronic transitions are reconstructed with time-dependent density functional theory (TD-DFT) and complete active space self-consistent field (CASSCF) calculations. In addition, to explore the basic mechanistic and energetic requirements of the NAPT mechanism, extensive theoretical calculations are performed on an isolated in-vacuum molecular model of DNBP.

2. Experimental and Theoretical Details

2.1. Synthetic Procedures. DNBP obtained from commercial sources (Avocado) was purified by column chromatography and doubly recrystallized from EtOH prior to the use. Large colorless parallelepiped crystals were obtained by slow evaporation from EtOH solution. The hydrochloride salt, 2-(2′,4′-dinitrobenzyl)-pyridinium chloride (DNBP·HCl), was obtained as colorless crystals by evaporation of the EtOH solution of DNBP with a slight excess of HCl. The *N*-methylated DNBP, 2-(2′,4′-dinitrobenzyl)-*N*-methylenamine, was prepared according to a literature method.[37]

2.2. Polarized Optical Spectra. The polarized optical spectra were recorded in transmission mode at ambient temperature from a single crystal ($0.7 \times 1.0 \times 1.1$ mm^3) colored by short and direct exposure to sunlight. Filtered output from a halogen lamp, cut by an aperture and passed through polarizer with an adjustable polarization angle, was focused onto the static single crystalline sample. After cutting low-wavelength region with a sharp-cut filter (L-42), the transmitted beam was focused onto an optical input of a monochromator coupled with a CCD detector. The spectra were calibrated and individually background-corrected. The intensity at single selected wavelengths is plotted in the polar plots. The identity of the spectra measured at the same polarization angle before and after the experiment confirmed that the thermal decay of the **NH** form during the experiment was negligible.

2.3. Theoretical Calculations. Most of the theoretical calculations were performed with the *Gaussian*98 program suite[38] running on a SGI Origin2000 supercomputer. Several additional optimizations were performed with the *Gaussian*03 version. Among the possible conformations, ground-state single-molecular models which are geometrically close to the **CH**

structure in the crystal were chosen and optimized[39] at HF/MP2/B3LYP[40,41]/B3PW1[42,43] levels using 6-31G, 6-31G(d,p), 6-31++G(d,p), and cc-pVT-ζ[44,45] model functions.

From the manifold of aci-nitro structures **OH**, two isomers are especially important for the reaction in the crystal and will be paid special attention here: **OH1**, with the OH group pointing toward the benzylic carbon atom, and **OH2**, with the OH group pointing toward the pyridyl nitrogen atom. Where feasible, polarization functions were supplied in order to extend the proton wave functions and to describe the transients with a partly bound and relatively distant proton. From the models tested, the B3LYP and B3PW1 three-parameter hybrid methods proved to be the best compromise between the costs and the requirements. The **CH**, **NH**, and **OH1** structures were thus optimized at the B3LYP/6-31+G(d,p) level. The B3PW91 and B3LYP/6-311+G(2d,p) single point energies were corrected for the scaled zero-point energy (ZPE). Due to the slight overestimation of the N−O bonds, the attempts to optimize the **OH2** structure with correlated methods always resulted in the **NH** structure. Therefore, the **OH2** structure was optimized at the HF/6-31++G(d,p) level. All minima were confirmed with subsequent vibrational analyses. The Synchronous Transit-Guided Quasi-Newton (STQN) method with the B3LYP/6-31++G(d,p) model chemistry was used to locate transition structures of the ground-state reactions among **CH**, **NH**, and **OH** other than those corresponding to simple donor-hydrogen bond stretching. The Internal Reaction Coordinate (IRC) scans were typically performed for 12, 50, or 70 points in both directions from the TS, at the step sizes of 0.05 or 0.03 amu$^{-1/2}$ Bohr, recalculating the force constants at the beginning of each run.

The time-dependent density functional theory[46,47] was employed to calculate the minimum-energy conformers and the transition states (TSs) between the three closed-shell isomers of DNBP. The Configuration Interaction-Singles (CIS) method,[48] the time-dependent Density Functional Theory (TD-DFT),[46,47] and the Complete Active Space Multiconfiguration SCF (CASSCF) method[49,50] were used to calculate the ground-state and excited-state electronic structures. The CIS method failed to reproduce satisfactorily the experimental transition energies. For the CASSCF calculations, the molecular orbitals near to the frontal orbitals that remain partially occupied during the excitation were selected and used to construct the active space for each DNBP isomer. The calculation performance allowed extension of the active space up to 8 electrons in 8 orbitals. The final active spaces consisted of the following molecular orbitals (in order of increasing energy): **CH**: 64, 62, 63, 67 (HOMO), 68 (LUMO), 69, 73, 74; **NH**: 64, 63, 66, 67 (HOMO), 68, 69, 73, 75; **OH1**: 60, 61, 66, 67 (HOMO), 68 (LUMO), 71, 70, 69; **OH2**: 64, 65, 66, 67 (HOMO), 68 (LUMO), 71, 72, 69.

3. Results

3.1. The Electronic Structure of DNBP Isomers. That the blue color ($\lambda_{EtOH} = 570$ nm, $\lambda_{solid} = 600$ nm) of photoirradiated DNBP owes to intramolecular charge transfer in **NH** was confirmed by comparison with the quaternized model, the colorless hydrochloride salt DNBP·HCl ($\lambda_{solution,solid} < 250$ nm),[51] and the quaternized/conjugated model, the blue-violet *N*-methyl **NH** ($\lambda_{solution} \approx 560$ nm). Accordingly, the electrostatic potential maps (Figure 1) show considerable charge separation in **NH** relative to **CH**, with the pyridinium and the dinitrophenyl rings carrying the excess positive and negative partial charges, respectively.

Figure 2 represents the polarized spectra recorded with the probe beam normal to two faces of a blue single crystal of

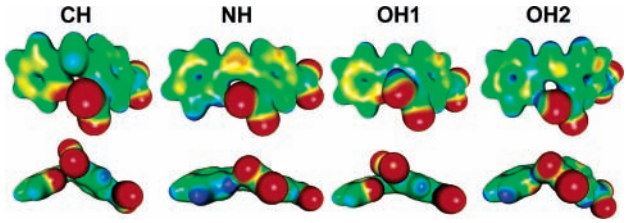

Figure 1. Molecular isosurfaces of the theoretical structures of **CH**, **NH**, and the two most probable conformers of **OH** (**OH1**, with the aci-nitro proton pointing to the benzylic carbon, and **OH2**, with the aci-nitro pointing to the pyridyl nitrogen), color-coded with the electrostatic potential. The value of the potential increases from red (most negative), through yellow and green to blue (most positive).

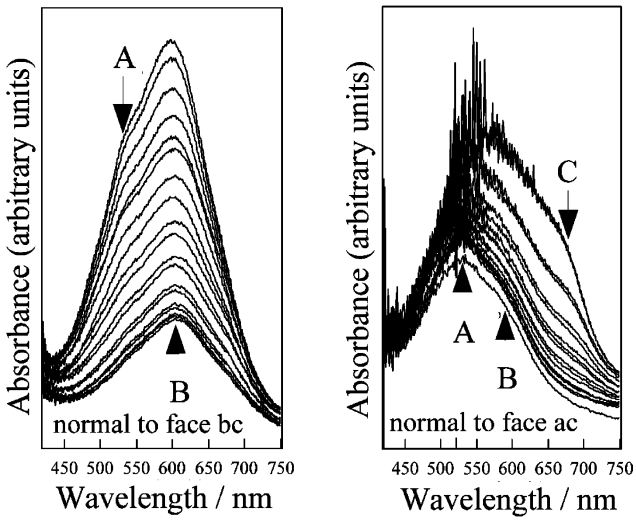

Figure 2. Angle dependence of the linearly-polarized optical absorption spectra of a blue single crystal of DNBP at room temperature. The different curves correspond to absorption at different angles between the orientation of the electric field of the incident light and an axis of the laboratory coordination system. The partial saturation of the spectra with large absorption in the case ⊥**ac** is a result of the low optical transparency of the crystal in that case.

DNBP.[52] Due to the angle-dependence of an overlapped absorption doublet at 535−545 nm (band A) and 600−605 nm (band B) and an additional weak absorption at 670 nm (band C) in the case ⊥**ac**, under linearly-polarized light photocolored single crystals of DNBP turn from blue to violet ⊥**ab** and ⊥**ac**, and from dark blue to light blue-green ⊥**bc** (**a**, **b**, and **c** are crystal axes parallel to the respective cell axes *a*, *b*, and *c*). As the **CH** form is optically transparent in the 420−750 nm region, the **OH** form has decayed ($t_{1/2} \approx$ seconds) on the time-scale of the experiment, and the amount of the open-shell species is insufficient to be detected in the electronic spectrum, bands A, B, and C are assigned to the longest-lived ($t_{1/2} \approx$ hours) isomer **NH**. The intensity change of the bands A and B at a fixed wavelength (Figure 3) shows that the color alteration ⊥**ac** is caused by a change in the overall absorption intensity, while the color change ⊥**bc** is caused by a change in the relative intensity of the two bands. From the TD-DFT calculation of the 10 lowest excited states (Table 1), the bands A and B are assigned to the $S_0 \rightarrow S_2$ excitation of **NH** from the HOMO to the three LUMOs, while the band C is prescribed to the $S_0 \rightarrow S_1$ excitation of **NH**[53] from the HOMO to the two LUMOs (S_0, S_1, and S_2 denote the ground state and first and second excited state, respectively). The relevant orbitals (Figure 4) confirm that excitation of the A/B doublet is related to charge transfer from the electron-rich allyl-pyridinium part to the electron-deficient

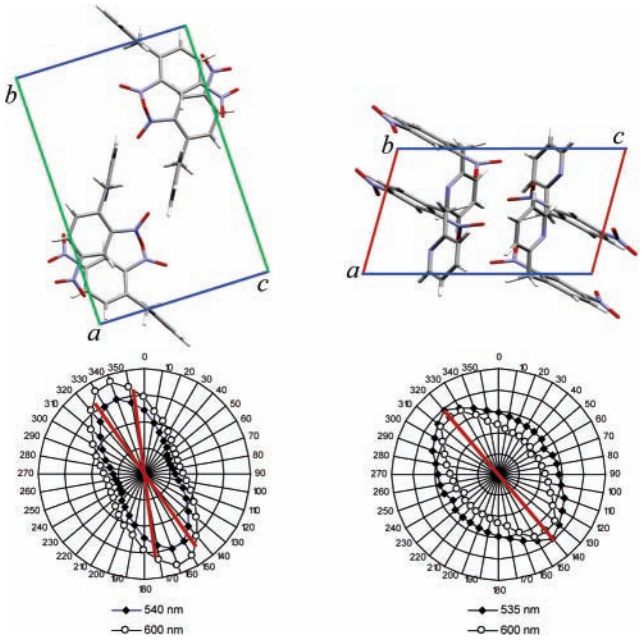

Figure 3. Top: molecular orientation of **CH** in the crystal viewed normal to two crystal faces. Bottom: polar plots of the intensities of band A (535−545 nm) and band B (600−605 nm) in the spectra recorded with the incident beam normal to the crystal faces bc (left) and ac (right). The wavelengths of the plotted intensities are indicated below the plots.

dinitrophenyl ring. The overlap of the dipole moment vectors μ of the bands A and B (Figure 3), their identical decay rates, the angle-dependence of the absorption maxima ($\approx$800 cm^{-1} for $\perp$**ac**), the appearance of a singlet band at an intermediate position (570 nm) in solution instead of the A/B doublet, and the large molar absorption coefficient of the model compounds for the **NH** form[54] all suggest that the A/B doublet is a result of the resonance-split transition $S_0 \rightarrow S_2$. Similarly with **CH**,[26] application of the selection rule to **NH** in the parent centrosymmetric crystal of **CH** ($P2_1/c$, $Z = 4$) implies activity of two quadruplet components, $A_g \rightarrow A_u$ (polarized $||b$ axis) and $A_g \rightarrow B_u$ (polarized $||ac$ plane). The average split (1920 cm^{-1}) is large, but comparable to that (3000 cm^{-1})[26] reported for **CH**. The "O" and "8"-like appearances of the cumulative polar plots $\perp$**ac** [overlapped $\mu(S_0 \rightarrow S_2)$ projections] and $\perp$**bc** [centrosymmetric $\mu(S_0 \rightarrow S_2)$ projections] correspond with packing of the dinitrophenyl chromophores over a center of symmetry and a 2-fold screw axis (2_1), respectively.[28,29]

3.2. Ground-State Closed-Shell Isomers of DNBP. The potential energy surface (PES) of DNBP includes closed-shell and open-shell reactions. The open-shell reactions, although contributing to the reactivity of DNBP by latent photochromism and photofatigue, are of small yield and complex chemistry[22] and will be the subject of another study. The closed-shell PT reactions of DNBP are initially induced by photoexcitation of **CH** but later proceed by thermal activation on the ground-state PES (Scheme 1). Moreover, there is a report on the thermochromic activity of a oNBP compound.[55] It is of interest, therefore, to start the theoretical modeling of the PT of DNBP with calculations on the ground-state thermal reactions.

The effect of the model chemistry on the S_0 theoretical structure of DNBP was tested on the **NH** form whose molecular conformation, and particularly the inter-ring dihedral angle, was shown to be the most method-sensitive. Selected theoretical parameters obtained using various methods are deposited as Supporting Information (Table S1). Generally, in the case of the HF methods the molecular conformation and the deviation

TABLE 1: Experimental and Theoretical Positions, Intensities, and Assignment of the Three Lowest-Energy Transitions of CH, NH, and OH

	λ_{calc}/nm[a]	oscillator strength f	λ_{exp}/nm	relevant contributing excitations
		CH Form		
$S_0 \rightarrow S_1$	335 (3.7)	0.01115	300−400[b]	HOMO-7 → LUMO+1
				HOMO-6 → LUMO
				HOMO-6 → LUMO+1
				HOMO-3 → LUMO+1
				HOMO-2 → LUMO
				HOMO-2 → LUMO+1
				HOMO-1 → LUMO
				HOMO-1 → LUMO+1
				HOMO → LUMO
				HOMO → LUMO+1
$S_0 \rightarrow S_2$	333 (3.7)	0.0006	300−400[b]	HOMO-5 → LUMO
				HOMO-5 → LUMO+1
$S_0 \rightarrow S_3$	329 (3.8)	0.0104	300−400[b]	HOMO-6 → LUMO+1
				HOMO-2 → LUMO+1
				HOMO-1 → LUMO
				HOMO-1 → LUMO+1
				HOMO → LUMO
				HOMO → LUMO+1
		NH Form		
$S_0 \rightarrow S_1$	529 (2.3)	0.0710	670	HOMO → LUMO
				HOMO → LUMO+1
$S_0 \rightarrow S_2$	453 (2.7)	0.5709	600−605[c]	HOMO → LUMO
			535−545[c]	
			(570[d])	HOMO → LUMO+1
				HOMO → LUMO+2
$S_0 \rightarrow S_3$	392 (3.2)	0.0698		HOMO → LUMO+2
		OH Form (the **OH1** Rotamer)		
$S_0 \rightarrow S_1$	541 (2.3)	0.0688	637[e]	HOMO → LUMO
				HOMO → LUMO+1
$S_0 \rightarrow S_2$	422 (2.9)	0.3116	435	HOMO-1 → LUMO
				HOMO → LUMO+1
$S_0 \rightarrow S_3$	375 (3.3)	0.0659		HOMO-2 → LUMO
				HOMO-1 → LUMO
				HOMO-1 → LUMO+1
				HOMO → LUMO+1

[a] The values in brackets are given in eV. [b] The lowest transitions of **CH** are weak and overlapped into an absorption in the 300−400 nm region. [c] Split into two bands. The maximum varies with the polarization angle. [d] In ethanol. [e] Observed for DNBP dispersed in polymer films.[26]

of the nitro group from the phenyl ring are strongly influenced by the basis set, while in the case of correlated methods (MP2, DFT) the effect of the basis set on the overall conformation and the torsion angle of the nitro group is relatively smaller. If only the HF results are considered, addition of polarization and diffuse functions leads to a larger angle between the *ortho*-nitro group and the phenyl ring. From the employed methods, the DFT and MP2 methods were found to yield, respectively, the strongest and the weakest conjugation (the smallest and the largest torsion angle) of the nitro group with the rest of the molecule. The geometries of the final set of isomers with stable wave functions were optimized without restraints, and the (all-real) frequencies were analytically computed at the B3PW91/6-31G(d) level. The B3PW91/6-311+G(2d,p) and B3LYP/6-311+G(2d,p) single point energies of the optimized structures were also calculated. The choice of the B3PW91 method was based on its ability to reproduce the experimental data for 2-nitrotoluene.[56] The B3LYP method was employed with the purpose of comparison with results on similar structures and assessment of performance of the two exchange functionals.

The optimized structures and TSs are presented in Figure 5, and the respective energies are listed in Tables 2 and 3. The structures **CH5** and **NH**[111] are close to the structures of the **CH** and **NH** forms in the crystal of DNBP.[29] For convenience,

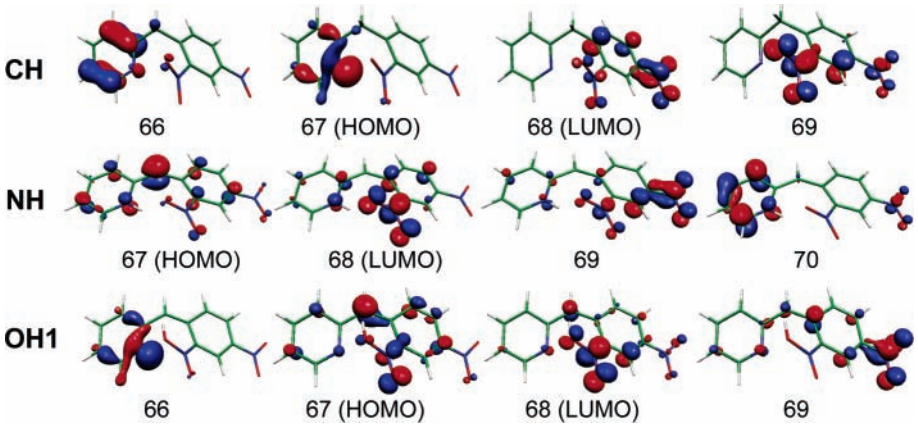

Figure 4. Plots of the relevant molecular orbitals in the optimized structures of **CH**, **NH**, and **OH** (the **OH1** isomer with the aci-nitro proton pointing toward the benzylic carbon atom is shown).

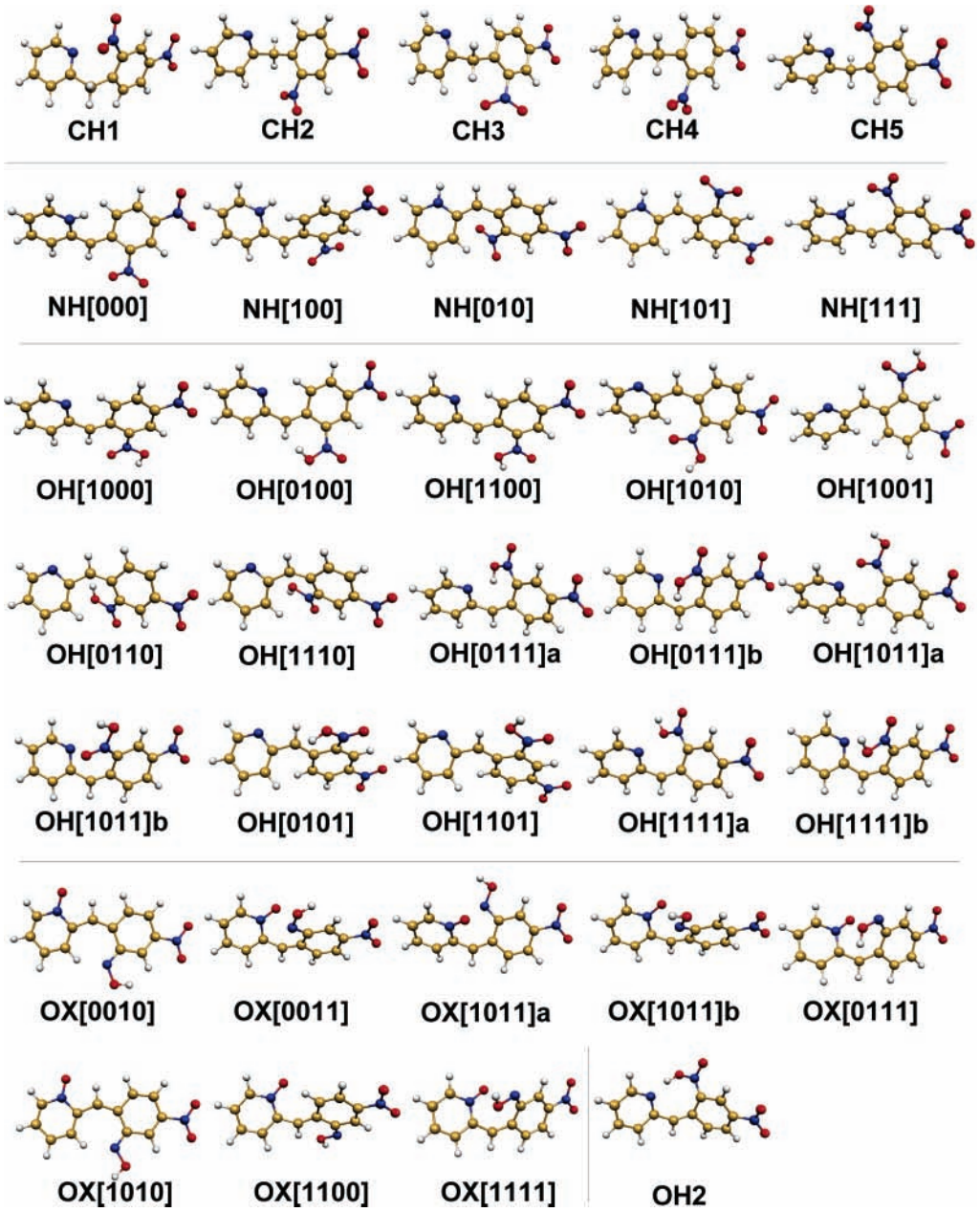

Figure 5. Theoretical minima of the DNBP isomers optimized at the B3PW1/6-31G(d) level. The structure of **OH2** optimized at the HF/6-31++G(d,p) level is also shown for comparison.

the conformations of **NH** and **OH** are labeled with three and four 1/0 digits, respectively. The first and the fourth digit denote syn/anti positions of the aci-nitro hydrogen atom (in respect to the other *ortho*-nitro oxygen) and the 2-pyridyl ring (the N atom

TABLE 2: Theoretically Calculated Single-Point Energies of the Closed-Shell Isomers of DNBP

isomer[a]	B3PW91/6-31G(d)// B3PW91/6-31G(d)	ZPE	sum ZPE+ electronic	B3PW91/6-311+ G(2d,p)// B3PW91/6-31G(d)	B3LYP/6-311+ G(2d,p)// B3PW91/6-31G(d)	B3LYP/6-311+ G(2d,p) (+sZPE)[b]
			CH Isomer			
CH1	−927.2972565	0.204633	−927.092624	−927.5633914	−927.9302336	**−927.7302662**
CH2	−927.2978113	0.204799	−927.093012	−927.5638028	−927.9308018	**−927.7306722**
CH3	−927.2987884	0.204795	−927.093994	−927.5643585	−927.9314437	**−927.7313180**
CH4	−927.2978113	0.204799	−927.093012	−927.5637772	−927.9308018	**−927.7306722**
CH5	−927.2972565	0.204633	−927.092623	−927.5633615	−927.9302070	**−927.7302396**
			NH Isomer			
NH[000]	−927.2759692	0.204927	−927.071042	−927.5459160	−927.9122700	**−927.7120154**
NH[100]	−927.2759692	0.204926	−927.071043	−927.5459165	−927.9118286	**−927.7115750**
NH[010]	−927.2701466	0.204651	−927.065491	−927.5401612	−927.9066960	**−927.7067114**
NH[101]	−927.2753084	0.204939	−927.070370	−927.5448498	−927.9111743	**−927.7109079**
NH[111] (**NH1**)	−927.2762082	0.204953	−927.071255	−927.5453740	−927.9121155	**−927.7118355**
			OH Isomer			
OH[1000]	−927.2586342	0.203405	−927.055229	−927.5299330	−927.8985992	**−927.6998319**
OH[0100]	−927.2453429	0.203360	−927.041983	−927.5167563	−927.8836898	**−927.6849665**
OH[1100]	−927.2522138	0.203464	−927.048750	−927.5228035	−927.8913291	**−927.6925041**
OH[1010]	−927.2492224	0.203109	−927.046113	−927.5213221	−927.8901222	**−927.6916441**
OH[1001]	−927.2526880	0.203229	−927.049459	−927.5248106	−927.8934180	**−927.6948226**
OH[0110]	−927.2401959	0.203017	−927.037179	−927.5131320	−927.8795874	**−927.6811992**
OH[1110]	−927.2439391	0.203066	−927.040873	−927.5167105	−927.8849308	**−927.6864947**
OH[0111]a (**OH1**a)	−927.2427017	0.203143	−927.039558	−927.5152787	−927.8815699	**−927.6830586**
OH[0111]b (**OH1**b)	−927.2427017	0.203144	−927.039558	−927.5153321	−927.8816099	**−927.6830976**
OH[1011]a	−927.2500453	0.203069	−927.046976	−927.5224687	−927.8909163	**−927.6924773**
OH[1011]b	−927.2500453	0.203069	−927.046976	−927.5224956	−927.8909377	**−927.6924987**
OH[0101]	−927.2408480	0.203185	−927.037663	−927.5130051	−927.8795452	**−927.6809928**
OH[1101]	−927.2474624	0.203398	−927.044065	−927.5192231	−927.8875613	**−927.6888008**
OH[1111]a (**OH3**a)	−927.2459551	0.202998	−927.042957	−927.5181572	−927.8864592	**−927.6880895**
OH[1111]b (**OH3**b)	−927.2459551	0.202998	−927.042957	−927.5181573	−927.8864593	**−927.6880897**
OH2		0.203		−927.5153899[c]	−927.8798035[d]	**−927.6768035**
			OX Isomer			
OX[0010]	−927.2247725	0.202720	−927.022052	−927.4963167	−927.8652572	**−927.6671592**
OX[0011]	−927.2251743	0.202724	−927.022450	−927.4963975	−927.8651528	**−927.6670509**
OX[1011]a	−927.2347720	0.203230	−927.031542	−927.5061943	−927.8758739	**−927.6772775**
OX[1011]b	−927.2347720	0.203230	−927.031542	−927.5061934	−927.8758132	**−927.6772169**
OX[0111]	−927.2259277	0.202908	−927.023019	−927.4980823	−927.8658632	**−927.6675815**
OX[1010]	−927.2346845	0.203406	−927.031279	−927.5060604	−927.8751693	**−927.6764009**
OX[1100]	−927.2310749	0.203315	−927.027760	−927.5032555	−927.8735618	**−927.6748824**
OX[1111]	−927.2321979	0.203269	−927.028929	−927.5044953	−927.8742695	**−927.6756351**

[a] Labels a and b denote mirror isomers of the same compound. [b] Scaled with 0.9772. [c] Single point energy calculated at the B3PW91/6-311+G(2d,p)//cc-pVT-ζ level. [d] Single point energy calculated at the B3LYP/6-311+G(2d,p)//cc-pVT-ζ level.

TABLE 3: Single-Point Energies of the Final Set of Transition State Structures

TS code	terminal structures[a]		B3PW91/6-31G(d)// B3PW91/6-31G(d)	ZPE	sum ZPE+ electronic	B3PW91/6-311+ G(2d,p)// B3PW91/6-31G(d)	B3LYP/6-311+ G(2d,p)// B3PW91/6-31G(d)	B3LYP/6-311+ G(2d,p) (+sZPE)[b]
					NH↔NH			
TS5	**NH**[101]	**NH**[000]	−927.2401916	0.202923	−927.037268	−927.5121178	−927.8785556	**−927.6802593**
TS6	**NH**[100]	**NH**[101]	−927.2401916	0.202924	−927.037268	−927.8785556	−927.5121177	**−927.3138204**
TS7	**NH**[100]	**NH**[111] (**NH1**)	−927.2452077	0.203633	−927.041575	−927.5168212	−927.8825574	**−927.6835673**
					OH↔OH			
TS8	**OH**[0110]	**OH**[1110]	−927.2324572	0.201780	−927.030677	−927.5059114	−927.8742845	**−927.6771051**
TS9	**OH2**a	**OH**[0111]a (**OH1**a)	−927.2419766	0.202482	−927.039495	−927.5145668	−927.8809843	**−927.6831189**
TS10	**OH2**b	**OH**[0111]b (**OH1**b)	−927.2419756	0.202486	−927.039489	−927.5145712	−927.8810120	**−927.6831427**
TS11	**OH2**a	**OH**[1111]a	−927.2457098	0.202574	−927.043135	−927.5174844	−927.8856019	**−927.6876466**
					CH↔OH, CH↔NH			
TS1	**CH**[c]	**NH**[101]	−927.2107543	0.198388	−927.012366	−927.4803417	−927.8436342	**−927.6497694**
TS2	**CH**[c]	**NH**[c]	−927.2086808	0.198469	−927.010212	−927.4788666	−927.8425352	**−927.6485913**
TS3	**CH5**	**OH**[0111]a (**OH1**a)	−927.2347630	0.199104	−927.035659	−927.5054725	−927.8692156	**−927.6746512**
TS4	**CH**[c]	**OH**[0101]	−927.2348769	0.198806	−927.036071	−927.4749497	−927.8695086	**−927.6752354**

[a] The labels a and b denote mirror isomers of the same compound. [b] sZPE stands for B3PW91/6-31G(d) zero-point energy correction scaled by 0.9772. [c] The IRC pathway branches to the rotational degrees of freedom. The likely terminal structures were determined by comparison with the optimized structures.

with respect to the *ortho*-nitro group), whereas the second and the third digit refer to the *Z*/*E* isomerism at the C=N and C=C bonds, respectively, as illustrated in Chart 1.[57] According to this notation, the **OH1** structure is identical with the **OH**[0111] structure, while the **OH2** structure corresponds to an intermediate between the **OH**[0111] and **OH**[1111] structures. As **OH2** could not be modeled well with the DFT (vide infra), for comparison the B3LYP/6-311+G(2d,p) and B3PW91/

CHART 1: Isomer (Left) and Atom (Right) Labeling Conventions

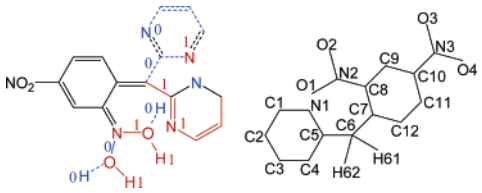

6-311+G(2d,p) energies of **OH2** optimized using the cc-pVT-ζ basis functions were also computed (Table 3).

As expected from several types of possible isomerism—tautomerism (by PT among **CH**, **OH**, and **NH**), cis−trans isomerism (around the double bonds in **OH** and **NH**), and rotational isomerism (around the single bonds in all three isomers), the preliminary HF/STO-3G examination of the closed-shell reactions of DNBP showed the rather complex S_0 PES. Subsequent detailed exploration at the B3PW91/6-31G(d) level afforded 5 stable minima of each of the **CH** and **NH** forms and 15 minima of the **OH** form. Starting from the **OH** structures, an additional 8 minima of an oxime *N*-oxide structure (**OX**) were obtained.[58] For three structures, **OH**[0111], **OH**[1111], and **OH**[1011], pairs of degenerate mirror isomers were located (labeled a and b henceforward). Due to the very small activation energy for rotation of the aci-nitro group, no stable minima with the employed method were obtained for the structures of **OH**[0010], **OH**[0001], **OH**[0000], and **OH**[0011].

The most difficult point during the theoretical construction of the S_0 PES was the modeling of the **OH** isomer, the highest-energy of the three closed-shell forms. The large conformational freedom of the aci-nitro group turns the **OH** form into a multitude of high-energy and relatively flat minima with small barriers for **OH↔OH** isomerization. Of these, at least three isomers are probable to exist in the crystalline state: **OH1** (**OH**[0111]), in which the proton of the aci-nitro group points toward the benzylic carbon and which probably exists shortly after the proton abstraction, **OH2**, with the dynamic proton pointing toward the pyridine nitrogen, which is assumed to exist before the delivery of the proton to the acceptor, and **OH3** (**OH**[1111]), with the proton pointing "outwards" (see below). **OH2** was successfully optimized at HF/6-31G(d,p), HF/6-31++G(d,p), HF/cc-pVT-ζ, and MP2/6-31G[59] levels, starting from the SCF-optimized geometry. Due to the slight overestimation of the N−O bonds by the DFT, however, all attempts to include the correlation effects in the optimization of **OH2** through the B3LYP/6-31++G(d,p) or BLYP, B1LYP, B3LYP, B3PW9, and SVWN methods with the 6-31G(d) basis always resulted in a downhill slide of the proton to the nearest lower-energy local minimum, **NH1** (**NH**[111]). The **OH2** structure represents a very shallow method-dependent local minimum on the reaction coordinate. This feature, as it will be discussed later, is critical for the feasibility of the PT in DNBP.

3.3. Ground-State Reactions of DNBP. Basic structural requirements for the occurrence of PT in the solid state are donor−acceptor proximity and collinearity of the donor/acceptor groups with the dynamic proton.[60] A unique feature of the NAPT mechanism is that, due to the mediation by the *ortho*-nitro group, the PT is possible even in the cases of unfavorable geometry. To unravel the structural requirements of the NAPT, the PT reactions of DNBP were theoretically studied at three levels: relaxed PES scans, IRC, and CASSCF calculations.

Relaxed scans[61] of the S_0 PES starting from each of the **CH**, **OH**, and **NH** forms with structures close to the structure of **CH** in the crystal showed that due to the unfavorable geometry (e.g., the sharp angle ∠(C−H- - -N) = 40° in DNBP), sole stretching of the C−H bond in **CH** does not result in any of the other two tautomers (Figure S1, deposited). Contrary, the **NH** and **OH** forms of similar conformation can interconvert simply by stretching of the respective donor-hydrogen bonds. The resulting parameters for the **NH→OH** reaction are E_a = 16.4 kcal mol^{-1} and $d^{\ddagger}$(N−H) = 1.197 Å, and for the **OH→NH** reaction E_a = 1.9 kcal mol^{-1} and $d^{\ddagger}$(O−H) = 1.120 Å, with the **NH** structure being about 12.8 kcal mol^{-1} more stable than **OH**. This result is in agreement with the experimental results (Scheme 1) and indicates that the thermally induced PT from **CH** is not likely but requires photoexcitation. Once some of the photoexcited **CH** is formed and has decayed to the ground-state **OH**, by small thermal activation of the O−H bond stretching vibration, the ground-state **OH** form can decay to the **NH** form. The thermal conversion of **NH** to **OH** is also possible but requires larger thermal activation.

To include the contribution of the molecular bending modes to the PT, the intramolecular isomerization of each of the closed-shell forms **CH**, **OH**, and **NH** was investigated with the IRC method. The search for TSs with the STQN method starting from the B3PW91/6-31G(d) minima afforded 3 unique TSs[62] for the **CH↔CH** isomerization and 7 unique TSs for the **NH↔NH** isomerization. In the case of the **OH↔OH** isomerization, the 15 (k) optimized **OH** minima required TS search along 105 ($k(k-1)/2$) possible pathways, which was computationally unaffordable to us. As the primary goal of the present study was modeling of the reactions similar to those in the solid state, the search was limited to a set of minima with Z configuration of the exo-C=C bond (Chart 1), that is, to the **OH**[$mn1p$] (m, n, p = 0, 1) structures, assuming that the $Z-E$ isomerization around this bond is highly improbable. The resulting 9 isomers required 36 TS searches, which resulted in 16 unique TSs used to describe the **OH↔OH** isomerization. The final IRC inspection afforded the 4 TSs connecting real **OH** minima. All TSs for conformational isomerization of the three closed-shell species are listed in Table 3, and the respective TSs are presented in Figure 6.

Next, the PT reactions among **CH**, **NH**, and **OH** were studied. In many occasions the QST2/QST3 runs between different structures converged to identical TSs. The real product/reactant pair in such a case was chosen on the basis of subsequent IRC analyses. The initial exploration of all 25 (5^2) possible reactions **CH↔NH** afforded 10 unique TSs. Due to the large number of **OH** minima, only the pathways probable in the crystal, that is, those between **OH**[mn11]a,b and **NH**[111]/**NH**[010], were investigated for the reaction **NH↔OH**. The 12 searches afforded 9 unique TSs. Similarly, for the reaction **CH↔OH** only the pathways between **OH**[mn11]a,b and **CH5**/**CH1** were considered, because **CH5** represents also **CH3** and **CH4** (e.g., the latter can be obtained by rotations of the *ortho*-nitro group and/or the pyridine ring of **CH5**) and **CH1** accounts also for **CH2** in the sense of the relative orientation of the *ortho*-nitro and methylene groups. The **CH↔OH** TS search afforded 5 unique TSs. From the overall of 24 TSs found for the PT reactions, two had identical structures, so that a set of 23 TSs with single imaginary frequencies was obtained. Six TSs showed RHF→UHF instability with RHF−UHF splits in the range 0.6−15.4 kcal mol^{-1} calculated on the RHF-optimized structures. The respective pathways were subsequently investigated as unrestricted singlets with the UB3PW91 STQN method. All unrestricted searches but one ended in diradicals with conformations similar to the respective closed-shell species. Only 2 of these open-shell structures were stable singlet diradicals (UB3PW91). The

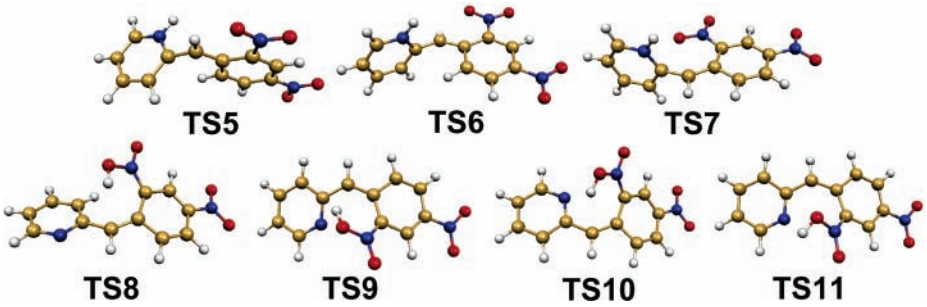

Figure 6. Optimized structures of the transition states for ground-state conformational isomerization of **CH**, **NH**, and **OH**.

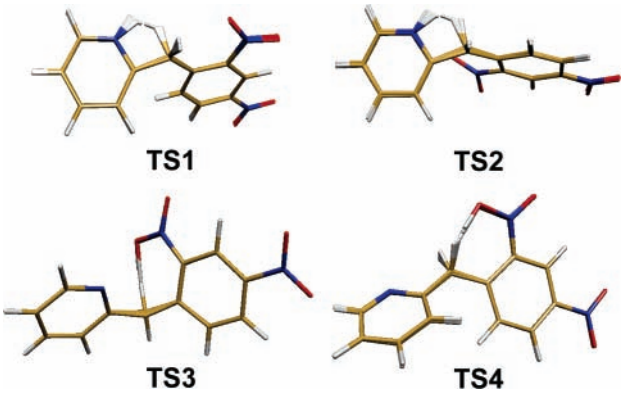

Figure 7. Overlapped representations of the IRC pathways of the ground-state PT reactions in DNBP around the transition states **TS1**−**TS4**. **TS1** and **TS2** correspond to the **CH↔NH** reaction, and **TS3** and **TS4** correspond to the **CH↔OH** reaction. The series of molecular conformations connecting **TS3** with **CH** and **OH** is the most similar with the conformation of the **CH** form in the crystal.

resulting set consisted of 6 stable singlet ground-state TSs, 2 singlet diradicaloid TSs on open-shell pathways, and a single second-order saddle point structure.[63] The IRC analysis ultimately confirmed that four TSs connect real minima. The PT pathways are represented as overlapped structures in Figure 7. The energies and geometrical parameters are listed in Tables 3 and 4. Animations of the PT reactions including the four TSs are deposited as Supporting Information.

The structures **TS1** and **TS2** relate **CH** and **NH** minima, whereas **TS3** and **TS4** connect **CH** and **OH** minima. The angles N1−C5−C6−C7 and C5−C6−C7−C8 in Table 4 show that the orientation of the phenyl and pyridine rings of **TS1** and **TS2** is very different from the **CH** form in the crystal (compare **TS1** and **TS2** in Figure 7 with **CH5** in Figure 5), suggesting that a direct reaction **CH↔NH** in the ground state is not probable without rotation of one of the aromatic rings (Figure 7).[64] For example, the **TS1** structure connects the **NH**[101] structure with a **CH** minimum. The PES scans of the intramolecular rotations around the single bonds of **CH** showed that in order to convert this **CH** minimum into **CH5** (the structure in the crystal), in the case of a single molecule, the molecule should be supplied with three additional energy portions of $E_a = 0.6$, 2.7, and 0.4 kcal mol^{-1} along a two-minimum pathway for rotation of the benzyl group around C6−C7. On the other hand, the similarity of the nitro−benzyl−pyridyl geometry, the phenyl−pyridine angle, and the *ortho*-nitro−phenyl angle of **TS3** and **CH** (Table 4) indicates that the reaction **CH↔OH** is easily possible in the crystal by rotation of only about 18.4 and 5.6° around the bonds C5−C6 and C6−C7, respectively, especially if the nitro group is excited to larger librations. The small rotation needed for the **CH↔OH** reaction is confirmed by the small activation energy for the thermal decay **OH→CH**, calculated from Tables 2 and 3 for **OH1**a and **CH5** as $E_a = 5.3$ kcal mol^{-1}. Although small rotation is required, the energy barrier for the reverse reaction **CH→OH** is still large at $E_a = 34.9$ kcal mol^{-1}. Most of this energy is spent for the homolytic dissociation of the C−H bond, and only a small part is used for the ring rotation.

TABLE 4: Distances (Å) and Angles (°) in the CH Structure in the Crystal and the Calculated Transition States for PT among CH, NH, and OH[a]

parameter	TS1	TS2	TS3	TS4	CH (exp)[29]
N1···H61	1.26	1.26	2.56	3.41	3.08
C6···H61	1.59	1.58	1.52	1.50	0.97
O1···H61	3.51	2.90	1.13	1.13	2.41
C6···N1	2.22	2.23	2.42	2.37	2.46
N1···O1	4.57	2.91	2.79	4.45	3.21
C6···O1	2.73	2.85	2.57	2.53	2.81
N1−C5	1.36	1.35	1.34	1.35	1.34
C5−C6	1.48	1.48	1.48	1.46	1.52
C6−C7	1.43	1.44	1.43	1.42	1.51
C7−C8	1.43	1.43	1.43	1.44	1.40
C8−N2	1.46	1.45	1.40	1.40	1.48
N2−O1	1.23	1.23	1.31	1.31	1.23
N1···H61···O1	141.2	77.7	89.4	153.9	70.5
O1···H61···C6	48.3	72.3	150.3	147.8	104.6
N1···H61···C6	101.8	102.3	67.5	36.6	42.9
C5−C6−C7	122.9	128.0	122.7	124.6	114.8
O1−N2−O2	123.3	123.6	118.0	118.1	124.0
N1−C5−C6−C7	−125.0	−129.7	23.0	−144.7	4.6
C5−C6−C7−C8	−168.4	25.9	−58.4	−159.4	−64.0
C6−C7−C8−N2	2.4	4.2	−22.0	17.4	−2.3
C7−C8−N2−O1	−8.2	21.4	2.3	−8.3	−30.2

[a] The labels refer to Chart 1. For the benzylic hydrogens, H61 denotes the dynamic (transferable) hydrogen atom.

From the calculated energies in Table 3 it is also inferred that although the manifold of **OH** isomers is for 4.3−19.5 kcal mol^{-1} (ZPE-corrected) less stable than the set of **NH** isomers, the energy barrier for PT from the methylene group to the *ortho*-nitro group is for 15.1−16.4 kcal mol^{-1} smaller than the transfer to the pyridyl nitrogen. This can be interpreted as a kinetic preference of the **OH** form over the **NH** form as a product of the PT from **CH**, despite the higher thermodynamic stability of the **NH** form. The small barrier for PT to the nitro group is apparently a result of the flexibility of the **OH** molecule. The large conformational freedom of the −N(O)OH group turns the **OH** isomer into a multitude of quasi-degenerate, flat minima. This is likely to be the crucial feature for the mediating role of the nitro group in the ground-state PT.

3.4. Excited-State Reactions of DNBP. The color change of DNBP and similar compounds is induced by UV radiation,[22] which means that the PT reactions are initiated from the excited state. The vertical excitations from **CH**, **NH**, **OH1**, and **OH2** to the first excited singlet and triplet states were modeled with the CASSCF(8,8)/6-31G(d) method (Figure 8, Table 5). The CASSCF model predicts correctly the energy order of the lowest singlet excitations $S_0 \rightarrow S_1$ in Table 1, **NH** (71.3 kcal mol^{-1}) <

TABLE 5: Theoretical Absolute (Hartrees) and Relative (kcal mol^{-1}) Energies of the Ground States and the Lowest Excited States at the CASSCF(8,8)/6-31G(d) Level[a]

	CH	NH	OH
S_0	−922.3137329937 (**0.00**)	−922.2413286359 (**0.00**)	−922.2417329532 (**0.00**)[b] −922.2568224502 (**0.00**)[c]
S_1	−922.1379927014 (**110.28**)	−922.1277537270 (**71.27**)	−922.1129814766 (**80.79**)[b] −922.0985225439 (**99.33**)[c]
T_1	−922.2080032967 (**66.35**)	−922.1375203170 (**65.14**)	−922.1936876051 (**30.15**)[b] −922.1833761602 (**46.09**)[c]

[a] The relative vertical excitation energies from the ground state are given in brackets in kcal mol^{-1}. The structures of **CH** and **NH** optimized at B3LYP/6-31++G(d,p) level. [b] The structure of **OH** optimized at B3PW91/6-31G(d) (minimum **OH**[0111]a, with the OH group oriented toward the bridging carbon C6) level was used (**OH1**). The excitation energies calculated for the degenerate mirror isomers **OH**[0111]a and **OH**[0111]b (as a test of the ability of the method to reproduce the energies) differed up to 0.02 kcal mol^{-1}. [c] The structure of **OH** optimized at HF/6-31++G(d,p) level, with the OH group oriented toward the pyridyl nitrogen N1 (**OH2**).

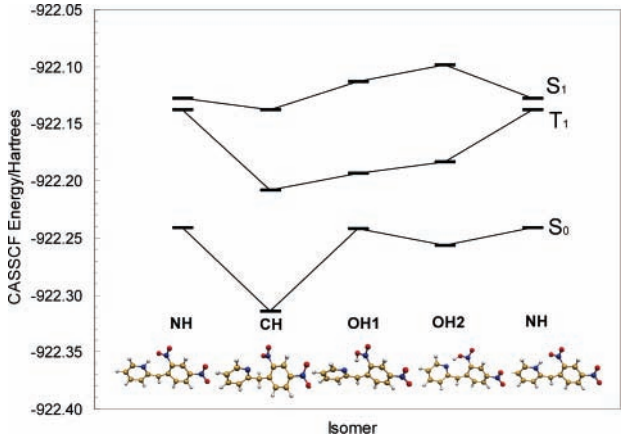

Figure 8. CASSCF(8,8)/6-31G(d) calculated transition energies to the lowest singlet and triplet excited states of the isomers **CH**, **NH**, and **OH**.

OH [**OH1** (80.8 kcal mol^{-1}) < **OH2** (99.3 kcal mol^{-1})] < **CH** (110.3 kcal mol^{-1}).

Figure 8 shows that in the S_1 state, **CH** is the most and **OH** is the least stable isomer. The energy difference between **CH** and **NH** (6.4 kcal mol^{-1}) in the S_1 state is smaller than in the S_0 state (45.4 kcal mol^{-1}). Similarly, the energy difference between **CH** and **OH** (15.7 and 24.8 kcal mol^{-1} for **OH1** and **OH2**, respectively) in the S_1 state is smaller than the respective difference in the S_0 state (45.2 and 35.7 kcal mol^{-1}). The excited-state PT is thus related to smaller energy differences. Another interesting feature of the S_1 energies in Figure 8 is that the large S_1 energy difference between **CH** and **OH2** (essential for the formation of **NH**, Δ = 24.8 kcal mol^{-1}) can be overcome by sequential transformation of **CH** to **NH** through **OH1** (Δ = 15.7 kcal mol^{-1}) and **OH2** (Δ = 9.1 kcal mol^{-1}). Therefore, in the case of excited-state PT, the **OH** form might play the same mediating role as in the ground state.

The CAS energies of the Franck−Condon states of **NH** indicate that the S_1 and the T_1 states have very close energies (Figure 8, Δ = 6.1 kcal mol^{-1}). This implies that avoided crossings or conical intersections may be present in the vicinity of the excited singlet **NH** which may result in singlet-to-triplet spin crossover.

4. Discussion

The previous experimental and theoretical results on DNBP and similar oNBP compounds have converged to the general reaction mechanism whose simplified form is presented in Scheme 1. The present study contributes to further understanding of the photophysics of DNBP with several new experimental and theoretical results. Although the calculations on a single molecule do not include the intermolecular interactions, it is well-known that they can still provide very accurate geometries and energies comparable to the experimental data, and in the case of the excited state calculations, they may be the only available method to obtain reliable description. The correspondence of the theoretical and experimental results, on the other hand, may be taken as an indication of similarity between the photophysics of oNBP compounds in the gaseous and solid states.

First, with the polarized absorption spectra it is confirmed, independently of the other experimental results, that the blue form of DNBP corresponds to the **NH** form which exists as oriented species in the single crystalline state. The blue color of **NH** originates from the second singlet electronic transition from the HOMO, located within the allyl-pyridinium part of the molecule, to the three lowest LUMOs which are spread over the dinitrophenyl fragment. The red shift of the absorption maximum of **NH** relative to **CH** is a result of the enhanced molecular conjugation of the **NH** form. Due to steric restrictions in the crystal the conjugation of the molecule in the solid state is less pronounced.

The experimental evidence for the reaction mechanism of solid oNBPs comes from the structure−activity relationships which correlate the photochromic activity with the crystal packing (polymorphism).[30,67] According to the packing-activity studies, there are at least three factors which govern the photochromic activity of a certain oNBP polymorph: (a) possible de-excitation channels opened by the eventual presence of $\pi-\pi$ stacking of the dinitrophenyl part (electronic factors),[65−67] (b) the ability of the *ortho*-nitro group to transfer the proton (steric factors) realized by its rotational freedom,[30] and (c) latent photochromism through the side radical reactions.[22] The relative importance of (a) and (b) for the solid-state photochromic activity is not certain, as there is a possibility that the photochromic activity is due to (c), that is, the irradiation may result in the creation of radicals which decay to the colored form. However, the clear correlation of the reaction cavity volumes for the nitro-assisted PT with the photoactivity of various oNBPs[30] confirmed that the rotational freedom of the nitro group is surely one of the decisive factors. According to the present theoretical analysis, due to the several possible types of isomerism, the flexible DNBP molecule in the fluid state possesses numerous degrees of freedom and has a complicated energy landscape comprised of at least 25 closed-shell minima. In the case of a single molecule, the flexibility enables the molecule to reach its geometry appropriate for PT, so that all oNBPs are photoactive in solution, although the colored species are of a short lifetime. In the solid state the molecule is fixed relative to its neighbors, and its conformational flexibility is reduced. The ring rotations are reduced to limited librations,

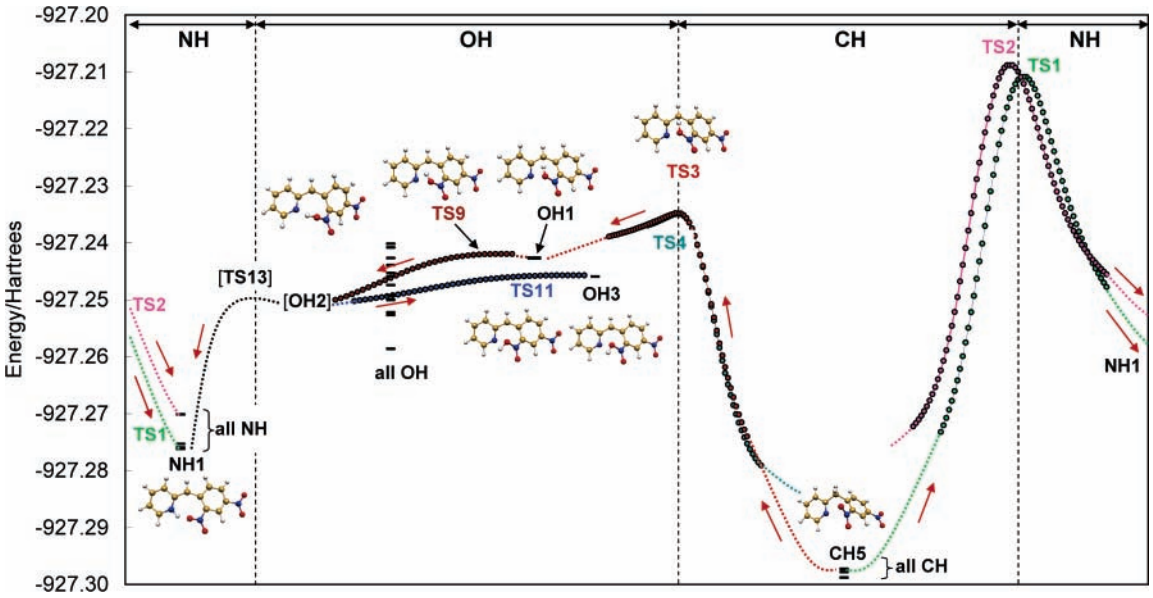

Figure 9. Slice of the ground-state potential energy surface of DNBP relevant for the nitro-assisted proton transfer and relative energies of all isomers. Structures **CH5**, **OH1** (identical with **OH**[0111]), **[OH2]**, **NH1** (identical with **NH**[111]), and **OH3** (identical with **OH**[1111]) are ground-state minima, while **TS3**, **TS9**, **TS11**, and [**TS13**] (hypothetical) are transition states which related them. The points obtained by the IRC analysis are presented as full circles connected to the related structures with dashed lines. The structures in square brackets could be optimized only with uncorrelated methods.

while the relatively large rotations of the smaller nitro groups are still retained. Therefore, in the solid state, in the case of a fairly proximate donor and acceptor, the photoactivity is determined by the ability of the nitro group to transfer the proton, that is, its rotational freedom and proximity with the donor and the acceptor.

In the case of the ground-state reactions, the calculations confirm that the thermal excitation of the C−H stretching mode in **CH** does not result in the reactions **CH↔OH** and **CH↔NH**. In addition to the C−H stretching, slight ring rotation is necessary for both reactions. In such a case, the **OH** form is thermodynamically less stable but the kinetically preferred product. Contrary, the **NH↔OH** isomerization can proceed in both ways simply by the stretching of the (N,O)−H bonds. Once created, **OH** can decay to **NH** with very small activation.

For a hypothetic ground-state NAPT from **CH**, the following series of events can be supposed (Figure 9): first, by supplying the ground-state **CH** form with energy of about 34.9 kcal mol^{-1} the benzylic proton which is closer to the nitro group is abstracted by the nitro group and the aci-nitro form **OH** is formed through the pathway **CH5→TS3→OH1**. The OH group then easily rotates toward the nitrogen atom through **OH1→TS9→OH2**, as the activation energy for this process is practically zero, and the molecule carries an excess of 5.3 kcal mol^{-1} from the previous process. One part of the **OH** form is then converted into the **NH** form through a transition structure which will be denoted **TS13**, through the pathway **OH2→TS13→NH1**. The rest of the **OH2** form may have its OH group rotated further and end up in another **OH** rotamer, **OH3**, with the proton pointing "outwards", through **OH2→TS11→OH3**. Subsequent thermal decay of this rotamer **OH3** back through the pathway **OH3→TS11→OH2→TS13→NH1** may result in delayed formation of **OH** and **NH**. This is possible due to the shallowness of the PES around **OH3**, which requires activation of only 0.3 kcal mol^{-1} ($< kT \approx 0.6$ kcal mol^{-1} at 300 K) to return back to **OH2** via **TS11**. It becomes clear that once the proton is abstracted by the nitro group, the small energy barriers related with the proton reorientation can be easily overcome, allowing the aci-nitro group to deliver it to the nitrogen acceptor. The high barrier for a direct proton jump from the carbon to the nitrogen, therefore, is replaced with a multistep process which is related with a more complex, but "softer" and more feasible energetic profile. This is due to the shallow, flat energy surface imposed by the rotational freedom of the *ortho*-nitro group of the aci-nitro form **OH**.

As mentioned above, the DFT methods were not able to model well the **OH2** isomer as well as **TS13**. Between **OH2** and **NH1** and particularly between **OH2** and **TS13** the PES is so flat that even a slight extension of the N−O bonds leads to a slide of the proton down to **NH1**. Testing of different methods was not helpful and lead to energies higher than the related transition states (Table 2). At the loosely defined minimum **OH2**, the PES branches to **NH1** (through **TS13**), **OH1** (through **TS9**), and **OH3** (through **TS11**). The fate of the proton will be ultimately decided by the vibrational mode which dominates in this state: enhanced O−H stretching will result in **NH**, while slight rotation around the N−O bond will result in either **OH1** or **OH3**.

As for the excited-state reactions, in principle, after the excitation of **CH**, the reaction can branch to de-excitation and PT in the excited state followed by de-excitation. The relative yield of these reactions will depend on the exact energy profile. The de-excitation brings the system back to the stable and nonreactive **CH** form. The excited-state calculations showed that in the excited state, **CH** is still the most stable isomer, but the energy difference with the other two isomers is much smaller than in the ground state. This is in agreement with the experimental data (Scheme 1), according to which reaction barriers for PT to **OH** and **NH** from the excited **CH** are 1 and 3 orders of magnitude smaller than for the respective ground-state reactions.[31,67] Therefore, the PT can occur in the excited state, in which case the OH group could have the similar mediating role as in the ground state. After **CH** has been converted to excited **OH** and the latter has decayed to the ground-state **OH**, the NAPT reaction proceeds in the same way as the ground-state process **OH→NH** explained above.

Acknowledgment. This study was performed through Special Coordination Funds for Promoting Science and Technology from the Ministry of Education, Culture, Sports, Science and Technology of the Japanese Government. P.N. acknowledges the academic scholarship granted by the Ministry of Education, Science, Sports and Culture (MEXT) of Japan.

Supporting Information Available: Potential surface scans (Figure S1), basis set effects (Table S1), fractional coordinates for DNBP·HCl (Table S2), the coordinates of the optimized structures and transition states, complete ref 38, crystallographic data for DNBP·HCl in CIF format, and animations of the PT reactions involving **TS1**−**TS4** in avi format. This material is free of charge via the Internet at http://pubs.acs.org.

References and Notes

(1) Fattah, J.; Twyman, J. M.; Heyes, S. J.; Watkin, D. J.; Edwards, A. J.; Prout, K.; Dobson, C. M. *J. Am. Chem. Soc*. **1993**, *115*, 5636.

(2) Wendeler, M.; Fattah, J.; Twyman, J. M.; Edwards, A. J.; Dobson, C. M.; Heyes, S. J.; Prout, K. *J. Am. Chem. Soc*. **1997**, *119*, 9793.

(3) Edwards, A. J.; Burke, N. J.; Dobson, C. M.; Prout, K.; Heyes, S. J. *J. Am. Chem. Soc.* **1995**, *117*, 4637.

(4) Maris, T.; Henson, M. J.; Heyes, S. J.; Prout, K. *Chem. Mater*. **2001**, *13*, 2483.

(5) Prout, K.; Heyes, S. J.; Dobson, C. M.; McDiad, A.; Maris, T.; Müller, M.; Seaman, M. *Chem. Mater*. **2000**, *12*, 3561.

(6) Heyes, S. J.; Dobson, C. M. *Magn. Reson. Chem*. **1990**, *28*, S37.

(7) Muller, M.; Edwards, A. J.; Prout, K.; Simpson, W. M.; Heyes, S. J. *Chem. Mater*. **2000**, *12*, 1314.

(8) Harada, J.; Ogawa, K. *J. Am. Chem. Soc.* **2001**, *123*, 10884.

(9) Harada, J.; Uekusa, H.; Ohashi, Y. *J. Am. Chem. Soc*. **1999**, *121*, 5809.

(10) McGeorge, G.; Harris, R. K.; Batsanov, A. S.; Churakov, A. V.; Chippendale, A. M.; Bullock, J. F.; Gan, Z. *J. Phys. Chem. A* **1998**, *102*, 3505.

(11) Ueda, Y.; Nakamura, N.; Chihara, H. *J. Phys. Soc. Jpn.* **1988**, *57*, 4063.

(12) Saito, K.; Yamamura, Y.; Kikuchi, K.; Ikemoto, I. *J. Phys. Chem. Solids* **1995**, *56*, 849.

(13) Saito, K.; Okada, M.; Akutsu, H.; Sorai, M. *Chem. Phys. Lett*. **2000**, *318*, 75.

(14) Galli, S.; Mercandelli, P.; Sironi, A. *J. Am. Chem. Soc*. **1999**, *121*, 3767.

(15) Riddell, F. G.; Arumugam, S.; Anderson, J. E. *J. Chem. Soc., Chem. Commun*. **1991**, 1525.

(16) Riddell, F. G.; Rogerson, M. *J. Chem. Soc., Perkin Trans*. **1996**, *2*, 493.

(17) Goc, R. *Z. Naturforsch. A* **1997**, *52*, 477.

(18) Bürgi, H.-B.; Blanc, E.; Schwarzenbach, D.; Liu, S.; Lu, Y.-J.; Kappes, M. M.; Ibers, J. A. *Angew. Chem., Int. Ed. Engl*. **1992**, *31*, 640.

(19) Blanc, E.; Restori, R.; Schwarzenbach, D.; Bürgi, H.-B.; Förtsch, M.; Venugopalan, P.; Ermer, O. *Acta Crystallogr*. *B* **2000**, *56*, 1003.

(20) (a) Corrie, J. E. T.; Trentham, D. R. In *Biological Applications of Photochemical Switches*; Morrison, H., Ed.; Wiley: New York, 1994; p 243. (b) Corrie, J. E. T.; Trentham, D. R. *"Caged Compounds", Methods in Enzymology*; Marriot, G., Ed.; Academic Press: New York, 1998. (c) Toscano, J. P. In *Advances in Photochemistry*; Neckers, D. C., von Bünau, G., Jenks, W. S., Eds.; Wiley: New York, 2001; Vol. 26, p 79.

(21) Houbrechts, S.; Clays, K.; Persoons, A.; Pikramenou, Z.; Lehn, J.-M. *Chem. Phys. Lett.* **1996**, *258*, 485.

(22) At cryogenic temperatures, the photochromic change is mainly caused by small yield of open-shell reactions that are induced by visible light and are mediated by a pair of photoinduced radicals: Naumov, P.; Ohashi, Y. *J. Phys. Org. Chem*. **2004**, *17*, 865.

(23) Hadjoudis, E. Tautomerism by hydrogen transfer in anils, aci-nitro and related compounds. In *Photochromism: molecules and systems*; Durr, H., Ed., Elsevier: 2003.

(24) (a) Sixl, H.; Warta, R. *Chem. Phys.* **1985**, *94*, 147. (b) Corval, A.; Kuldová, K.; Eichen, Y.; Pikramenou, Z.; Lehn, J. M.; Trommsdorff, H. P. *J. Phys. Chem*. **1996**, *100*, 19315.

(25) Casalegno, R.; Corval, A.; Kuldová, K.; Ziane, O.; Trommsdorff, H. P. *J. Lumin*. **1997**, *72*−*74*, 78.

(26) Shinohara, S.; Takeda, J.; Ooike, T.; Kurita, S. *J. Phys. Soc. Jpn.* **1999**, *68*, 1725.

(27) For DNBP and other examples, see: (a) Craig, B. B.; Atherton, S. J. *Proc. SPIE-Int. Soc. Opt. Eng*. **1984**, *482*, 96. (b) Margerum, J.; Miller, L.; Saito, E. *J. Phys. Chem*. **1962**, *66*, 2434. (c) Sousa, J.; Weinstein, J. *J. Org. Chem*. **1962**, *27*, 3155. (d) Wettermark, G. *J. Phys. Chem*. **1962**, *66*, 2560. (e) Wettermark, G.; Ricci, R. *J. Chem. Phys*. **1963**, *39*, 1218. (f) Wettermark, G.; Black E.; Dogliotti, L. *Photochem. Photobiol*. **1965**, *4*, 229. (g) Ault, A. *J. Chem. Educ*. **2000**, *77*, 1386. (h) Schwörer, M.; Wirz, J. *Helv. Chim. Acta* **2001**, 84, 1441.

(28) (a) Seff, K.; Trueblood, K. N. *Acta Crystallogr*. *B* **1968**, *24*, 1406. (b) Scherl, M.; Haarer, D.; Fischer, J.; DeCian, A.; Lehn, J.-M.; Eichen, Y. *J. Phys. Chem*. **1996**, *100*, 16175. Our XRD measurements showed that the crystal structure of DNBP in the range 77−298 K is identical with the published structure.

(29) Naumov, P.; Sekine, A.; Uekusa, H.; Ohashi, Y. *J. Am. Chem. Soc*. **2002**, *124*, 8540.

(30) (a) Naumov, P.; Ohashi, Y. *Acta Crystallogr*. *B* **2004**, *60*, 343. (b) Peskin, M.; Scherl, M.; Haarer, D.; Khatib, S. *J. Am. Chem. Soc*. **1997**, *119*, 7167.

(31) Sixl, H.; Warta, R. *Chem. Phys*. **1985**, *94*, 147.

(32) Ziane, O.; Casalegno, R.; Corval, A. *Chem. Phys.* **1999**, *250*, 199.

(33) Khatib, S.; Tal, S.; Godsi, O.; Peskin, U.; Eichen, Y. *Tetrahedron* **2000**, *56*, 6753.

(34) Andreev, G. N.; Schrader, B.; Hristozova, D. A.; Delchev, V. B.; Petrov, J. S.; Rademacher, P. *J. Mol. Struct*. **2003**, *645*, 77.

(35) Frank, I.; Grimme, S.; Peyerimhoff, S. D. *J. Phys. Chem*. **1996**, *100*, 16187.

(36) Frank, I.; Marx, D.; Parrinello, M. *J. Phys. Chem*. **1999**, *103*, 7341.

(37) Nunn, A. J.; Schofield *J. Chem. Soc*. **1952**, 583.

(38) *GAUSSIAN98* (rev. A11), Frisch, M. J. et al. Gaussian, Inc., Pittsburgh, PA, **1998**.

(39) Schlegel, H. B. *J. Comput. Chem*. **1982**, *3*, 214.

(40) Becke, A. D. *Phys. Rev. A* **1988**, *38*, 3098.

(41) Lee, C.; Yang, W.; Parr, R. G. *Phys. Rev. B* **1988**, *37*, 785.

(42) Perdew, J. P.; Chevary, J. A.; Vosko, S. H.; Jackson, K. A.; Pederson, M. R.; Singh, D. J.; Fiolhais, C. *Phys. Rev. B* **1992**, *46*, 6671.

(43) Perdew, J. P.; Burke, K.; Wang, Y. *Phys. Rev. B* **1996**, *54*, 16533.

(44) Peterson, K. E.; Woon, D. E.; Dunning, T. H. *J. Chem Phys*. **1994**, *100*, 7410.

(45) Wilson, A.; van Nourik, T.; Dunning, T. H. *J. Mol. Struct. (THEOCHEM)* **1997**, *388*, 339.

(46) Bauernschmitt, R.; Ahlrichs, R. *Chem. Phys. Lett*. **1996**, *256*, 454.

(47) Casida, M. E.; Jamorski, C.; Casida, K. C.; Salahub, D. R. *J. Chem. Phys*. **1998**, *108*, 4439.

(48) Foresman, J. B.; Head-Gordon, M.; Pople, J. A.; Frisch, J. M. *J. Phys. Chem*. **1992**, *96*, 135.

(49) Yamamoto, N.; Vreven, T.; Robb, M. A.; Frisch, M. J.; Schlegel, H. B. *Chem. Phys Lett*. **1996**, *250*, 373.

(50) Frisch, M. J.; Ragazos, I. N.; Robb, M. A.; Schlegel, H. B. *Chem. Phys. Lett*. **1992**, *189*, 524.

(51) Analytical data: Calcd for $C_{12}H_{10}N_3O_4Cl$: C, 48.74; H, 3.66; N, 14.21. Found: C, 48.49; H, 3.43; N, 14.42. IR (KBr)/cm^{-1}: 2610 ν(NH), 2439 ν(NH), 1611, 1535 $\nu(NO_2)$, 1344 $\nu(NO_2)$, 764. Crystallographic data for DNBP·HCl: 2-(2′,4′-dinitrobenzyl)pyridinium hydrochloride, $C_{12}H_{10}N_3O_4Cl$, $M_r = 295.68$, $T = 293(2)$ K, $\lambda = 0.71073$ Å, monoclinic, $P2_1/c$, $a = 9.9583(7)$ Å, $b = 5.7946(4)$ Å, $c = 23.2137(17)$ Å, $\beta = 101.697(2)°$, $V = 1311.71(16)$ Å^3, $Z = 4$, $\rho_{calc} = 1.497$ Mg·m^{-3}, $\mu = 0.308$ mm^{-1}, $F(000) = 608$, crystal size: $0.30 \times 0.05 \times 0.05$ mm^3, $GOF = 1.024$, $R_1[I > 2\sigma(I)] = 0.0591$, $wR_2[I > 2\sigma(I)] = 0.1229$, $R_1 = 0.1187$, $wR_2 = 0.1499$, largest peak/hole 0.277/−0.200 e·Å^{-3}. ORTEP diagrams of the molecular structure and the crystal structure viewed along the *b*-axis are deposited as Supporting Information (Figure S2). The pyridinium hydrogen and the chloride ion are connected with hydrogen bond d(N1···Cl1) = 3.036(3) Å, ∠(N1−H1···Cl1) = 162.8°.

(52) Due to the low signal/noise ratio, the spectra recorded ⊥**ab** are not discussed here.

(53) The assignment of band C (670 nm) rather than the doublet A/B (600−605 and 535−545 nm) to the lowest singlet transition of **NH** is consistent with the recent reassignment of a band at similar position (637 nm) to the lowest transition of **OH**[7] instead of the characteristic **OH** band (435 nm). Namely, the excited-state calculations show that the lowest singlet transitions of **NH** and **OH** should appear at close positions (calculated: 529 and 541 nm), and they should be much weaker than the respective second-lowest transitions (0.0710 compared to 0.5709 and 0.0688 compared to 0.3116).

(54) Wettermark, G.; Sousa, J. *J. Phys. Chem*. **1963**, *67*, 874.

(55) Corval, A.; Kuldova, K.; Eichen, Y.; Pikramenou, Z.; Lehn, J. M.; Trommsdorff, H. P. *J. Phys. Chem*. **1996**, *100*, 19315.

(56) Il'ichev, Y. V.; Wirz, J. *J. Phys. Chem*. *A* **2000**, *104*, 7856.

(57) Thus, for example **OH**[1011] represents **OH** tautomer with *syn*-H aci-nitro atom, *E*-C═N bond, *Z*-C═C bond, and *anti*-oriented pyridyl ring. Similarly, the reaction **OH**[1011]→**OH**[1001] represents cis−trans isomer-

ization around the C═C bond, and **OH**[1111]→**OH**[1011] designates a simple [1,3]H-shift between the two *ortho*-nitro oxygen atoms in **OH**.

(58) The oxime *N*-oxide structure **OX** does not contribute to the PT reactions and will not be discussed here. This molecule, however, may be involved in some of the photofatigue reactions.

(59) For the MP2/6-31G optimized structure, d(O−H) = 1.076 Å and d(N···H) = 1.449 Å.

(60) The proton transfer can be considered as a dynamic case of a series of hydrogen bonds, for which the collinearity is a necessary condition. For example, for C−H···O bonds ∠(C−H···O) = 110−180°: Desiraju, G.; Steiner, T. *The weak hydrogen bond*; Oxford Science Publications: New York, 1999; p 59.

(61) At the HF/6-31G(d,p) level. **NH**: starting d(N−H) = 1.0250 Å, increment Δd = 0.0191 Å; **OH**: d(O−H) = 0.9830 Å, Δd = 0.0195 Å; **CH**: d(C−H) = 1.093 Å, Δd = 0.01586 Å.

(62) The term "unique" TSs here refers to the number of different TSs for the specific reaction.

(63) During the TS search several condensed tricyclic structures were also obtained. IRC runs from these structures resulted in OH rotation, did not lead to any of the known DNBP isomers, and were omitted from the further analysis.

(64) Eventual fast flipping of the pyridyl ring is surely a possibility that should be considered in further studies. However, the photochromic activity of the 2,2′-bipyridyl and *ortho*-phenanthrolyl derivatives, where the acceptor is bulkier and the rotation is not probable, suggests that the dynamics of the pyridyl ring does not contribute significantly to the PT.

(65) Eichen, Y.; Lehn, J.-M.; Scherl, M.; Haarer, D.; Fischer, J.; DeCian, A.; Corval, A.; Trommsdorff, H. P. *Angew. Chem., Int. Ed. Engl*. **1995**, *34*, 2530.

(66) Khatib, S.; Botoshansky, M.; Eichen, Y. *Acta Crystallogr*. *B* **1997**, *53*, 306.

(67) Schmidt, A.; Kababya, S.; Appel, M.; Khatib, S.; Botoshansky, M.; Eichen, Y. *J. Am. Chem. Soc*. **1999**, *121*, 11291.